Article

Incorporation of Bentonite Mining Waste in Ceramic Formulations for the Manufacturing of Porcelain Stoneware

**Joabi Faustino Ferreira [1], Fabiana Pereira da Costa [1], Luiz Fhelipe Diniz Borborema [2],
Rafaela Reis de Arimateia [3], Raquel Santos Leite [1,2], Raira Chefer Apolinário [4], Haroldo Cavalcanti Pinto [4],
Alisson Mendes Rodrigues [1,2,*], Gelmires de Araújo Neves [1,3] and Romualdo Rodrigues Menezes [1,3]**

[1]   Graduate Program in Materials Science and Engineering (PPG-CEMat), Federal University of Campina Grande, Av. Aprígio Veloso-882, Bodocongó, Campina Grande 58429-900, PB, Brazil

[2]   Academic Unit of Materials Engineering, Science and Technology Center, Federal University of Campina Grande, Av. Aprígio Veloso-882, Bodocongó, Campina Grande 58429-900, PB, Brazil

[3]   Laboratory of Materials Technology (LTM), Department of Materials Engineering, Federal University of Campina Grande (UFCG), Av. Aprígio Veloso-882, Bodocongó, Campina Grande 58429-900, PB, Brazil

[4]   São Carlos School of Engineering—EESC, University of São Paulo—USP, São Carlos 13563-120, SP, Brazil

*   Correspondence: alisson_mendes@ymail.com

Abstract: Mining processes produce a massive amount of waste which, if not treated properly, can cause significant environmental and social impacts. Recently, some studies have focused on the use of mining waste as an alternative raw material. This work developed new sustainable ceramic formulations based on bentonite mining waste (BMW) for applications in porcelain stoneware. The BMW was incorporated into the ceramic masses in different percentages (0, 2.5, 5, 10, 15, 20, 25, and 40 wt.%), in partial replacement to feldspar and total to quartz. X-ray diffraction (XRD), differential thermal calorimetry (DTA), and thermogravimetry analysis (TGA) techniques were used to characterize bentonite waste. Samples (50 mm × 20 mm × 5 mm) were obtained by uniaxial pressing. Such samples were dried and sintered at 1150, 1200, and 1250 °C. The physical–mechanical properties (apparent porosity, water absorption, linear shrinkage, apparent density, and flexural strength) were evaluated for sintered samples. The phases formed after sintering treatments were characterized by XDR and scanning electron microscopy (SEM). The BMW presented a mineralogical composition suitable for use as ceramic raw material. In summary, our results presented that the new sustainable ceramic formulations sintered at 1250 °C have the potential for use in stoneware and porcelain stoneware.

Keywords: bentonite mining waste; ceramic masses; porcelain stoneware; physical–mechanical properties

1. Introduction

Over the years, mineral extraction has established itself as a significant activity for the world economy; because it contributes to the gross domestic product (GDP), generates jobs, and is a source of extra income for small rural landowners. According to data from the Brazilian Mining Institute (IBRAM), 2021 mineral production increased by 7% compared to 2020, from 1.01 million to 1.15 million tons in 2021. This increased the revenue of this sector in Brazil from BRL 209 billion to BRL 339 billion from 2020 to 2021 [1].

The northeast Brazilian region stands out for having a large part of the mineral reserves. Bentonite production, for example, is among the 10 most present and exploited minerals in northeastern Brazil. The economic importance of bentonites is due to their numerous industrial applications [2,3], such as use in cosmetics [4,5], pharmaceutical products [6,7], drilling fluids [8,9], as adsorbents [10,11], waterproofing dams and landfills [12], etc.

The main bentonite deposits in Brazil are located in the Paraíba state. This state holds about half of the national reserves and is responsible for more than 90% of the production of

raw bentonite in the country [13]. Figure 1 shows the map with the location of the Paraíba state and the geological map of Boa Vista city, where bentonite has been exploited for over 60 years.

Figure 1. Location of the Paraíba state and geological profile of Boa Vista city, where bentonite mining has taken place since 1961.

Bentonite is usually extracted by surface mining. Bentonite mines are covered by a layer of soil, varying from 1 to 10 m, and interspersed with layers of basalt. Excavators and tractor-scrapers remove the topsoil layers, subsoil, and the overburden of basalt above the clay. The overburden of basalt is removed and often inappropriately deposited in the environment. Although waste management, transport, treatment, and the final destination are their generators' responsibility [14,15], waste dunes are widespread near mining companies, with tons of materials remaining after bentonite extraction. The impacts of mineral activities become more relevant when there is no adequate destination for the waste, which can generate soil, water, and air contamination and destruction of the landscape, among others [16].

Given this scenario, studies on the reuse of mining waste have intensified in recent years to reduce the impacts caused by incorrect allocation. Numerous mining residues have been successfully reused as an alternative raw material to manufacture sustainable materials, such as ceramic refractories [17,18], ceramic tiles [19–21], bricks [22–26], roof tiles [27–30], porous ceramics [31–34], and sanitary ware [35], among others. Various mining waste types stand out, including iron ore tailings [36–38], kaolin waste [39,40], scheelite [41,42], ornamental rock waste [43,44], perlite waste [45–48], etc. In a recent study, Araújo et al. [49] evaluated the potential for reusing waste from bentonite mining as adsorbents for treating water contaminated with cationic dyes. The authors found that bentonite waste can also remove cationic dyes in wastewater.

Reuse studies of bentonite mining waste are still scarce. It is known that these wastes are generally composed of iron and sodium silicate, calcite, feldspar, and smectite [49], which makes it possible to use them as raw materials in ceramic industries. However, no

studies were found in the literature that reused bentonite mining waste as a raw material to manufacture ceramic products. In this work, new formulations of ceramic masses containing bentonite mining waste were incorporated, developed, and characterized to produce porcelain stoneware. The waste was subjected to chemical, physical, mineralogical, and thermal characterizations; and was incorporated into the ceramic masses in the partial replacement of feldspar and the total replacement of quartz. The effects of the different waste incorporation contents (0, 2.5, 5, 10, 15, 20, 25, and 40 wt.%) and the temperature of sintering (1150, 1200, and 1250 °C) in the physical–mechanical properties and mineralogical phases were evaluated.

2. Materials and Methods

2.1. Materials

Kaolin (Rocha Minérios, Juazeirinho-PB, Brazil), plastic clay, quartz, feldspar (Armil Mineração do Nordeste, Parelhas-RN, Brazil), and waste from bentonite mining (BMW). The BMW was collected from various locations in the mineral deposits of the União Nordeste Bentonita (BUN) industry, located in Boa Vista city, Paraíba, Brazil. The BMW samples were mixed by the quartering technique. The raw materials were characterized by X-ray fluorescence (Shimadzu, EDX 720) and X-ray diffraction (Shimadzu, XRD6000) using Cu-Kα radiation (40 kV/30 mA), 0.02° step, and a 2θ angle range of 5–60°. Differential thermal analysis (DTA) (BP Engenharia, RB-300) and thermogravimetric analysis (TGA) (Shimadzu, TA 60H) was performed under an atmosphere of air with a heating rate equal to 12.5 °C.min⁻¹. The laser diffraction (Cilas, 1064 LD) determined the BMW particle size distribution.

2.2. Sample Preparation, Sintering Treatments, and Characterizations

Different BMW contents (0–40 wt.%) were incorporated into the ceramic masses in total replacement to quartz and partial to feldspar. The nomenclatures for all ceramic formulations used in this work are listed in Table 1. The raw materials were sieved to 74 μm, moistened (7% moisture), and mixed at the ball mill at 450 rpm for 60 min. Samples (50 mm × 20 mm × 5 mm) were obtained from uniaxially pressed powders (Servitech Press, CT-335) at 13.5 MPa for 10 s (pre-pressing), followed by pressing at 50 MPa for 20 s. Then, the samples were dried in an oven for 24 h at 110 °C. The sintered treatments were performed with *Flyever* Equipamento equipped with Controller FE 50 RP for 40 min at different temperatures (1150, 1200, and 1250 °C). For all samples, a heating rate of 30 °C·min⁻¹ was used. Cooling occurred following the furnace inertia to room temperature (~24 °C).

Table 1. Nomenclature of the ceramic compositions investigated and the proportion (wt.%) of each raw material.

Formulations	Raw Materials (wt.%)				
	Kaolin	Plastic clay	Feldspar	Quartz	BMW
F1	23	27	35	15	0
F2	23	27	47.5	0	2.5
F3	23	27	45	0	5
F4	23	27	40	0	10
F5	23	27	35	0	15
F6	23	27	30	0	20
F7	23	29	23	0	25
F8	23	29	8	0	40

The water absorption (WA), apparent porosity (AP), and apparent density (AD) properties were measured by Archimedes' method [50]. The length of samples with and without heat treatment was measured to obtain linear shrinkage (LS) measurements. Shimadzu's universal mechanical testing machine (model Autograph AG-X 50 kN) was used for the

three-point flexural strength (FS). The load, distance between support, and test speed were 5 KN, 40.4 mm, and 0.5 mm·min^{-1}, respectively. Ten samples were used for each WA, AP, LS, and FS experiment. XRD experiments were accomplished to characterize the mineralogical phases after sintering treatment. SEM experiments were used to analyze the crystal morphologies.

3. Results and Discussion

3.1. Raw Materials (Chemical and Mineralogical Composition)

The chemical composition and the XRD patterns of the conventional raw materials (feldspar, plastic clay, quartz, and kaolin) and the BMW are shown in Table 2 and Figure 2, respectively. Kaolin and plastic clay presented SiO_2 (42.62% and 48.49%) and Al_2O_3 (36.51% and 38.14%) as major oxides. These oxides are associated with the tetrahedral and octahedral layers of the clay mineral kaolinite and free silica. Kaolinite (JCPDS 78-2110) was the main crystalline phase identified in these clays, followed to a lesser extent by quartz (JCPDS 46-1045) and mica (JCPDS 83-1808). The Fe_2O_3 contents were less than 3%, which indicates that the standard sample (without BMW) will probably show a light color after firing. Feldspar (JCPDS 84-0710), mica (JCPDS 83-1808), and quartz (JCPDS 46-1045) were the main mineralogical phases detected in feldspar. Due to the high content of K_2O (11.68%) detected, the raw material was classified as potassium feldspar. The main function of the alkalis present in the samples is to act as fluxes, favoring the formation of a glass phase [8].

Table 2. Chemical composition of the BMW, kaolin, plastic clay, quartz, and feldspar used in this work.

Samples	Oxides (wt.%)								
	SiO_2	Al_2O_3	Fe_2O_3	K_2O	MgO	CaO	TiO_2	Others	LOI *
BMW	44.61	12.35	15.06	0.30	4.15	5.66	2.10	0.27	15.50
Kaolin	48.49	38.14	0.34	0.78	NP **	0.07	NP **	0.15	12.03
Plastic clay	42.62	36.51	2.85	NP **	NP **	NP **	0.01	0.30	17.71
Quartz	91.84	3.66	0.12	0.90	NP **	0.14	NP **	0.40	2.94
Feldspar	61.03	19.26	NP **	11.68	NP **	NP **	NP **	0.59	7.44

* LOI: loss on ignition. ** NP: not present.

The main constituents of the BMW were SiO_2 (44.61%) and Al_2O_3 (12.35%). The high contents of Fe_2O_3 (15.06%), CaO (5.66%), and MgO (4.15%) are related to the iron silicate (JCPDS 17-0548), magnesium silicate (JCPDS 11 -0273), feldspar (JCPDS 22-687), and calcite (JCPDS 05–0086), evidenced by XRD (see Figure 2). The high content of Fe_2O_3 (15.06%) present in the BMW indicates that the samples with the waste showed a dark color after firing. Some evidence of the clay mineral smectite (JCPDS 29-1497) was detected in the BMW, which originates from the geological formation of bentonite.

3.2. Thermogravimetric Analysis of Raw Materials and Granulometry of the Bentonite Waste

The BMW showed a marked weight loss (12.7%) between 24 °C and 200 °C (Figure 3a), related to a loss of free and adsorbed water. The hydroxyl loss from clay minerals, a typical phenomenon of this raw material, was detected in the second stage of weight loss (2.0%), between 200 and 500 °C. The decomposing of the calcite mineral, which releases CO_2, was detected in the last stage (5.6%) and occurred between 500 °C and 1000 °C. The total weight loss was 20.3%. In the differential thermal analysis (DTA) curve, two endothermic events were identified: the first and, more intense, at approximately 70 °C is characteristic of the free water loss and the second, at about 640 °C, is due to the decomposition of the calcite present in the waste.
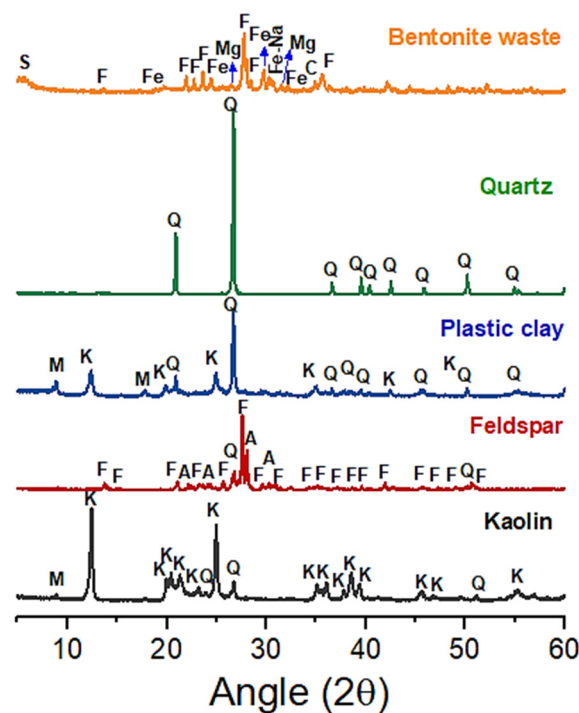
Figure 2. XRD patterns were measured from conventional raw materials (quartz, plastic clay, kaolin, and feldspar) and bentonite mining waste. F—feldspar, M—mica, C—calcite, K—kaolinite, Q—quartz, A—anorthite, S—smectite, Fe—iron silicate, Mg—magnesium silicate, Fe-Na—sodium iron silicate.

In the TGA/DTA curves of kaolin and plastic clay (Figure 3b,c) the following thermal transformations can be observed: two endothermic peaks related to the loss of free water (kaolin: ~52 °C, clay: ~106 °C) and of hydroxyls present in the structure of clays (kaolin: ~605 °C, clay: ~587 °C), and an exothermic peak (kaolin: ~975 °C, clay: ~985 °C) associated with mullite nucleation [17,32]. No transition was observed in the quartz (Figure 3d) and feldspar (Figure 3e) DTA curves. Kaolin, plastic clay, quartz, and feldspar showed a total mass loss of 16.1%, 10.9%, 2.8%, and 4.8%, respectively.

Figure 4 shows the normal and accumulated granulometric distribution curves of the BMW. Note that the normal distribution curve presents a bimodal behavior, i.e., the curve presents two maxima (approximately 11.2 μm and 89.3 μm). The BMW has the most considerable fraction of particles, with diameters above 20 μm (48.07% of accumulated volume), a medium particle diameter of 6.11 μm, $D_{10\%}$ = 2.18 μm, $D_{50\%}$ = 18.17 μm, and $D_{90\%}$ = 142.84 μm. These values are similar to those found in the literature for use in ceramic masses [17,35]. So, the BMW has an adequate granulometric distribution for use in ceramic mass.

3.3. Ceramic Mass Formulations (Chemical, Mineralogical Composition, and Thermal Behavior)

The chemical composition of the ceramic mass formulations without the BMW (F1) and with 2.5, 5, 10, 15, 20, 25, and 40 wt.% of the BMW (F2 to F8) are listed in Table 3. The SiO_2 (44.74 wt.%–55.62 wt.%) and Al_2O_3 (28.33 wt.%–30.60 wt.%) contents are similar for most formulations. These constituents are responsible for forming refractory phases during the sample sintering. The highest levels of fluxing oxides (Fe_2O_3 + K_2O + MgO + CaO) were observed for the formulations with the highest levels of the BMW (F6 (9.33 wt.%), F7 (9.30 wt.%) and F8 (11.59 wt.%)). Higher fluxing agent contents in the mass favor the liquid phase formation during firing. The presence of a liquid phase during the firing is very important as it contributes to the densification of the ceramic pieces. Furthermore, the liquid phase helps the diffusion of aluminum ions, benefiting the nucleation and growth of the mullite phase [17,41,51]. The XRD patterns (Figure 5) indicate that the BMW incorporation up to 40 wt.% did not cause significant changes in peak intensity or the ceramic masses'

mineralogical profile. Overall, the formulations presented quartz, kaolinite, feldspar, mica, and calcite crystalline phases.
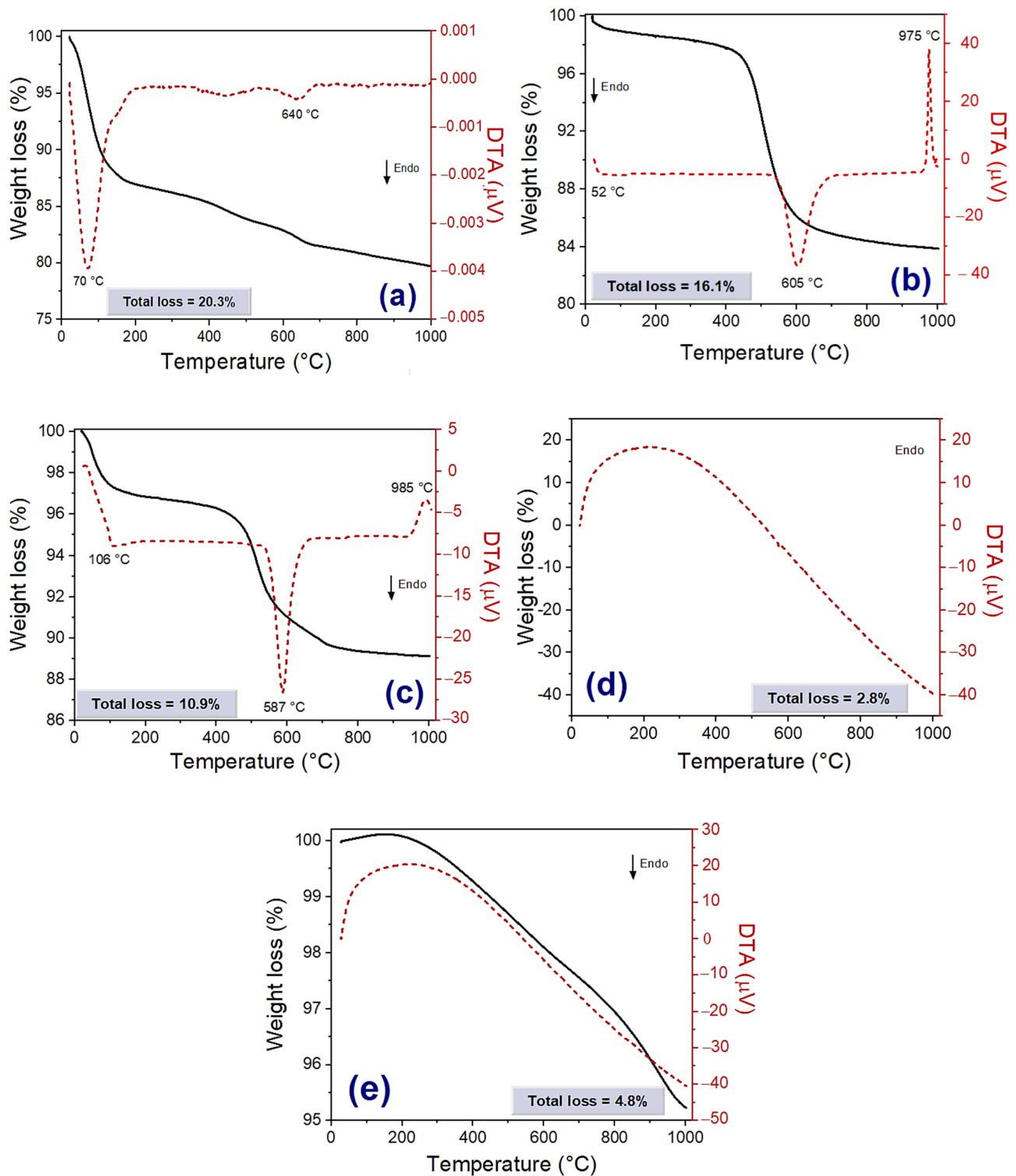

Figure 3. Curves of TGA and DTA of bentonite waste (**a**), kaolin (**b**), plastic clay (**c**), quartz (**d**), and feldspar (**e**).
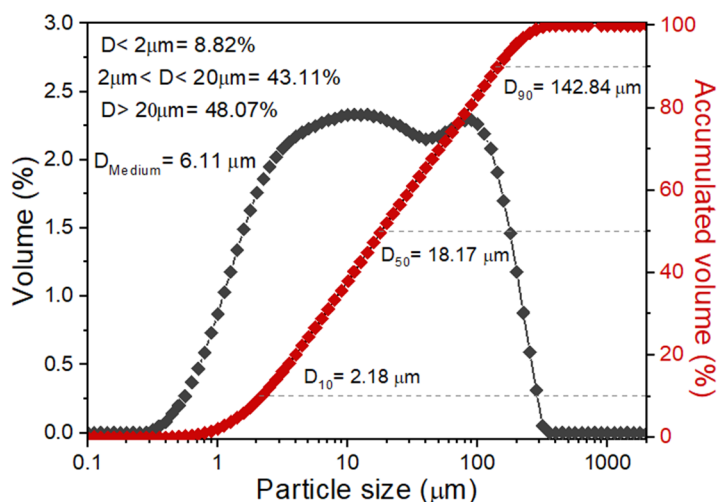
Figure 4. Normal and accumulated granulometric distribution curves obtained from the BMW.

Table 3. Chemical composition of ceramic mass formulations evaluated.

Formulations	Oxides (wt.%)								
	SiO_2	Al_2O_3	Fe_2O_3	K_2O	MgO	CaO	TiO_2	Others	LOI *
F1	55.62	28.33	0.86	4.42	NP **	NP **	0.18	0.29	10.30
F2	51.94	29.45	1.24	5.41	0.75	0.29	0.23	0.47	10.22
F3	49.86	30.01	1.64	3.77	0.83	0.69	0.32	1.10	11.78
F4	49.58	29.02	1.69	4.76	0.82	0.70	0.33	1.21	11.89
F5	47.86	30.48	2.73	3.51	0.95	1.32	0.42	0.18	12.55
F6	48.49	28.89	3.22	3.55	1.05	1.51	0.54	1.03	11.72
F7	47.08	30.60	3.92	2.60	1.15	1.63	0.60	0.46	11.96
F8	44.74	30.28	5.92	1.25	1.76	2.66	1.00	0.44	11.95

* LOI: loss on ignition. ** NP: not present.
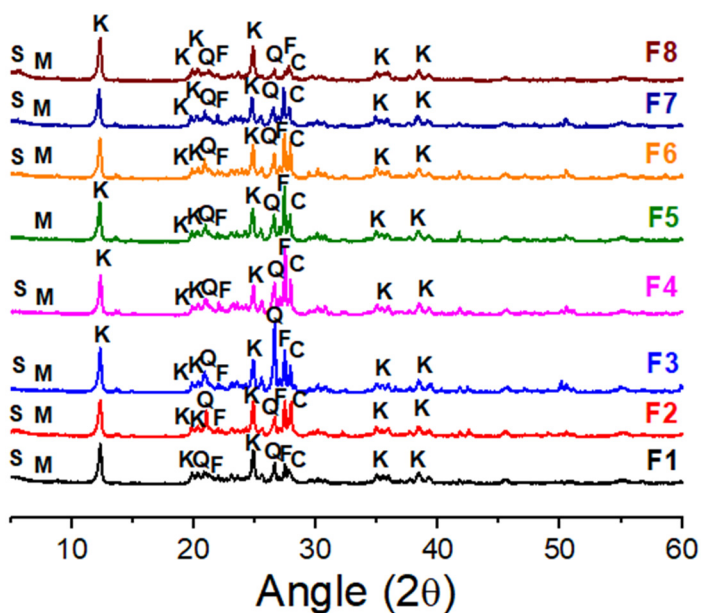
Figure 5. XRD patterns of standard ceramic mass (F1) and the ceramic masses containing the BMW (F2 to F8). S—Smectite, C—Calcite, Q—Quartz, M—Mica, K—Kaolinite, F—Feldspar.

Figure 6a,b show the TGA and DTA curves of the ceramic formulations containing the BMW (F2 to F8). In general, all formulations showed similar behavior. The total mass

loss (Figure 6a) varied between 9.7% and 13.8%, corroborating the LOI data presented in Table 3. An endothermic peak at approximately 58 °C was detected in Figure 6b. Such a peak corresponds to free water loss and adsorbed water. On the other hand, the intensity of the endothermic peaks around 500 °C is characteristic of the decomposition of the calcite present in the masses.
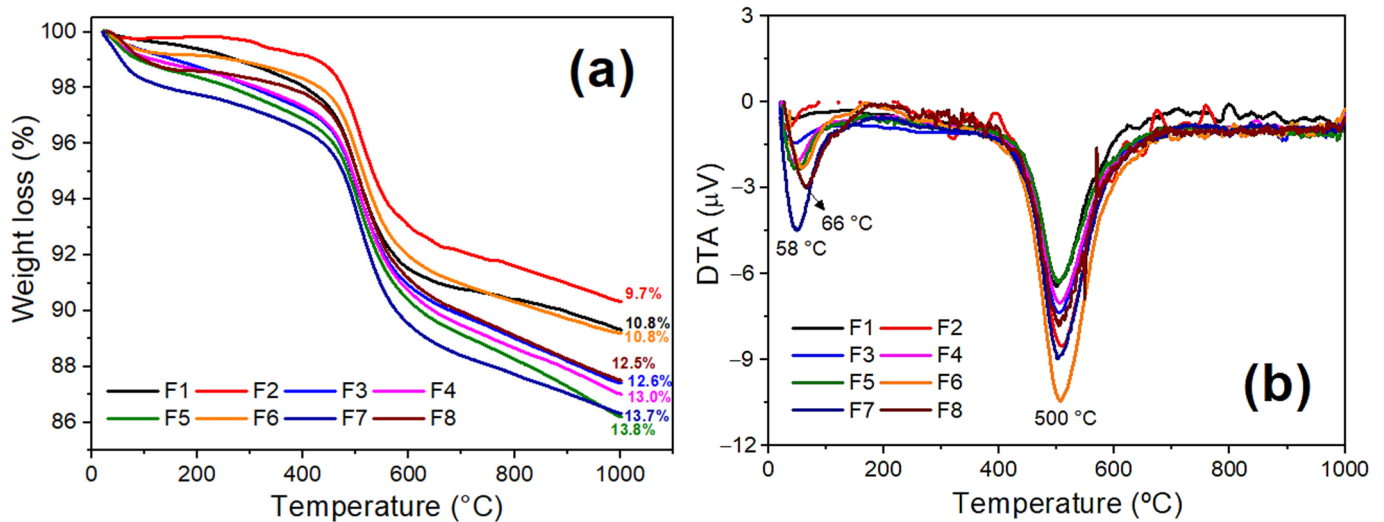
Figure 6. Curves of the TGA (**a**) and DTA (**b**) of the standard ceramic mass (F1) and the formulations containing the BMW (F2 to F8).

3.4. Sintered Samples (Physical and Mechanical Properties)

The Shapiro–Wilk and Levene tests analyzed data on physical and mechanical properties for normality and homoscedasticity, respectively. As the data differ significantly from a normal distribution ($p < 0.05$), the non-parametric Kruskal–Wallis test was used to verify if there were remarkable differences between the different content of bentonite waste incorporation and the sintering temperature. The Multiple Comparisons test was used to identify the samples that differed in cases where the Kruskal–Wallis test was significant. All analyses were performed using the Statistica® software version 14 (Data Science Workbench, Palo Alto, CA, USA).

Figure 7a–d show the LS, AP, WA, and AD results of the samples after the sintering step treatment (1150, 1200, and 1250 °C). In general, LS values ($p = 0.0069$) increase with increasing sintering temperature (Figure 7a). Such behavior is due to the forming of a liquid phase at higher temperatures favoring the diffusion process. The increase in the liquid phase formation during sintering tends to densification and, consequently, the shrinkage of the ceramic piece because the liquid phase penetrates the existing pores [51,52]. The samples containing the BMW (F2 to F8) showed the highest LS values compared to the sample without the BMW (F1) ($p = 0.0000$). This behavior can be attributed to the higher content of fluxing oxides of the bentonite waste ($Fe_2O_3 + K_2O + MgO + CaO = 25.17$ wt.%); see Table 2. However, in the samples with 2.5 to 15 wt.% of BMW (F2 to F5), the temperature increased from 1200 to 1250 °C and did not cause remarkable changes in LS values; this indicated that the highest liquid phase formation was reached at temperature of 1200 °C.
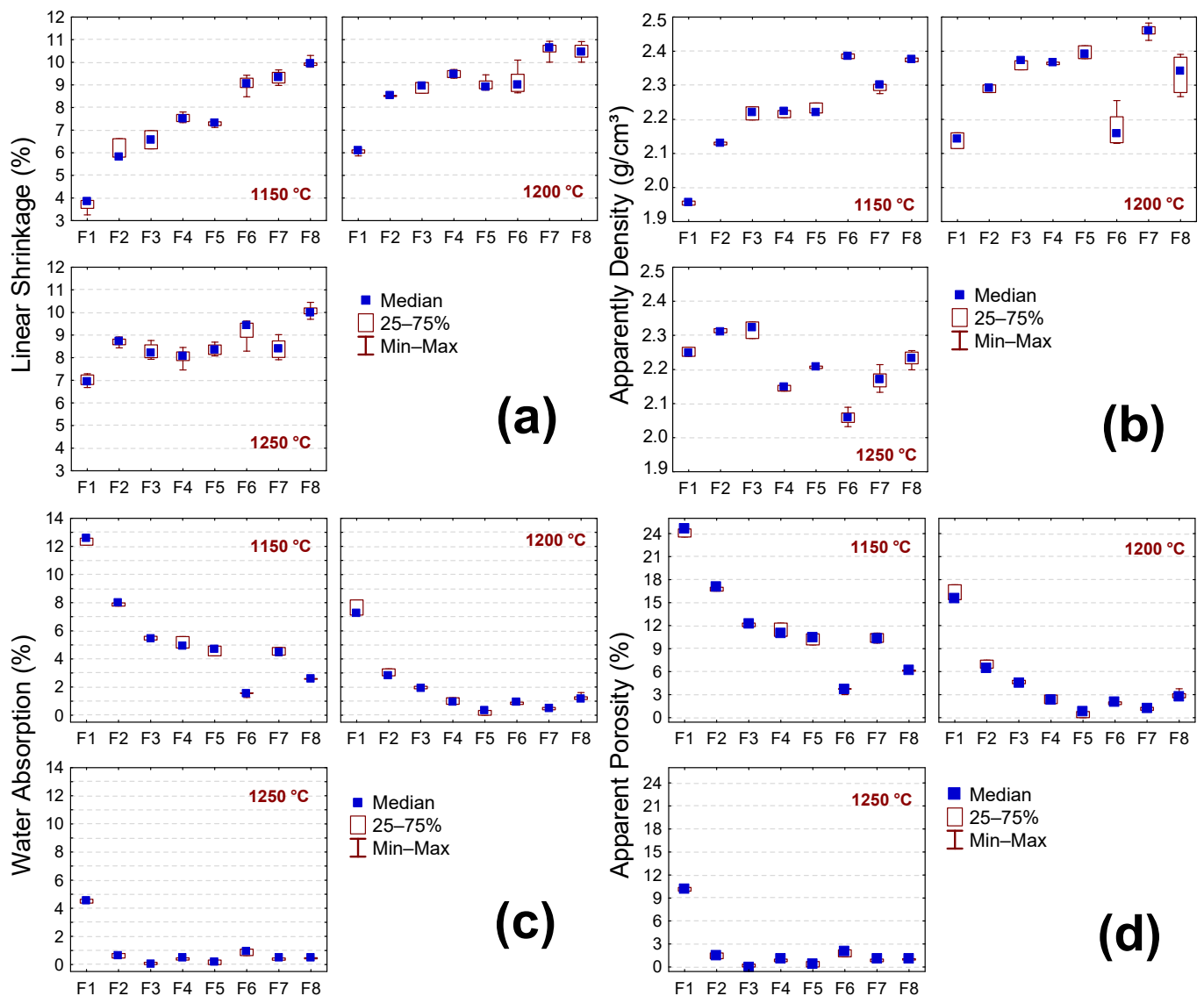
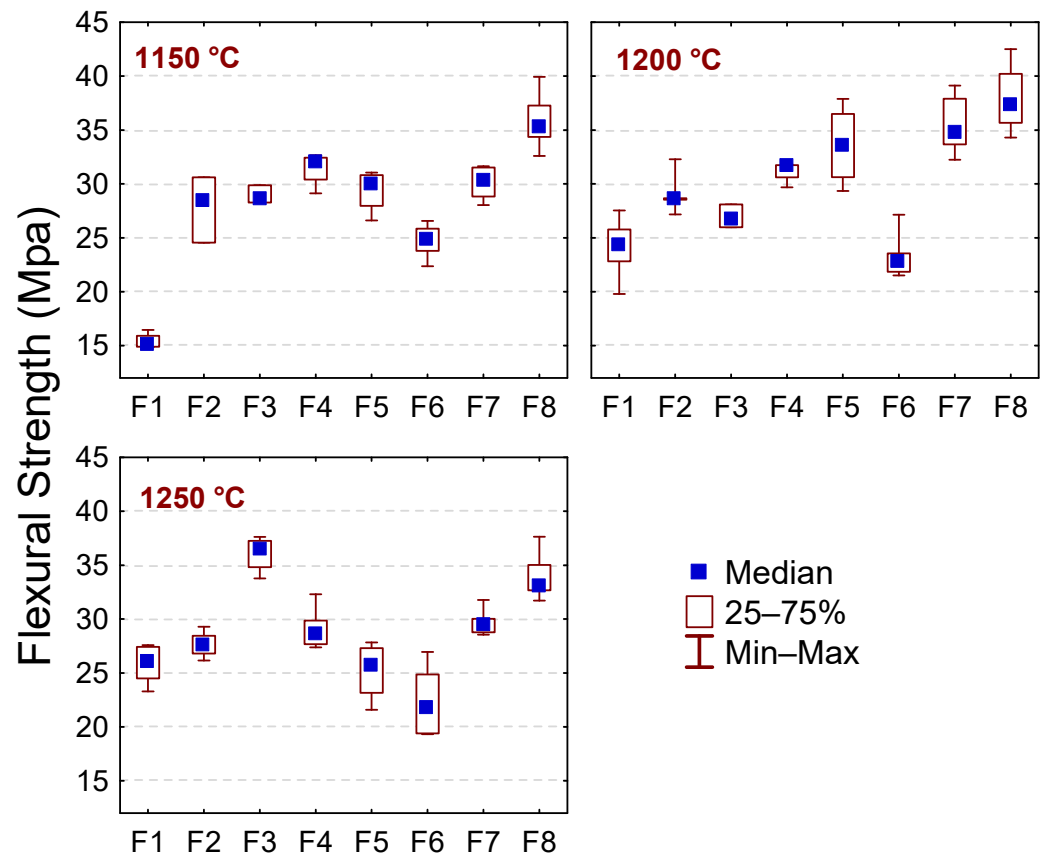**Figure 7.** Physical properties of the sample without the BMW (F1) and with 2.5, 5, 10, 15, 20, 25, and 40 wt.% of the BMW (F2 to F8), after sintering at 1150 °C, 1200 °C, and 1250 °C. (**a**) LS—Linear shrinkage, (**b**) AP—apparent density, (**c**) WA—water absorption, and (**d**) AP—apparent porosity.

The AD values (Figure 7b) increase when the temperature increases from 1150 to 1200 °C and tend to decrease from 1200 to 1250 °C. However, this difference was insignificant ($p = 0.0076$), suggesting that the effects of increasing temperature are less intense for sample density. On the other hand, the WA and AP values (Figure 7c,d) decreased with increasing sintering temperature ($p = 0.0000$). This was already expected since WA and AP are closely related to the amount of liquid phase formed. It is also noted that the incorporation of bentonite waste favored a decrease in the WA and AP values. Regardless of the sintering temperature, sample F1 (without the BMW) presented WA and AP values higher than the others (with waste) ($p = 0.0000$). These results indicate that the BMW can potentially replace quartz and part of feldspar in ceramic masses to manufacture ceramic tiles. The WA is an important parameter in the classification of ceramic tiles. Based on the ISO 13006 standard [53], the samples containing the BMW and sintered at 1200 °C present WA values suitable for application as stoneware (0.5% < WA < 3.0%), while those sintered at 1250 °C have the potential to be used as porcelain stoneware (WA ≤ 0.5%).

The flexural strength values (FS) increase with the incorporation of the BMW ($p = 0.0000$); see Figure 8. In general, the highest FS values (>30 Mpa) were observed in samples with

BMW contents above 15 wt.% (F5, F6, F7, and F8). When the temperature increases from 1150 to 1200 °C led to a significant increase in the FS values of the sample without the BMW (F1: from ~15.4 MPa to 24.1 MPa) (p = 0.0000), such behavior is attributed to the vitrification of the samples and the mullite phase formation that start to go nuclear around 980 °C [32,54]. Probably, at 1150 °C, the vitrification of the F1 sample was not facilitated well; this sample showed a high apparent porosity (~24%) (see Figure 7d), which indicates that the liquid phase formation was insufficient to promote the sample densification. Above 1200 °C, the formation of a liquid phase is probably more significant, favoring densification and consequently strengthening the material.

Figure 8. Flexural strength of the sample without the BMW (F1) and with 2.5, 5, 10, 15, 20, 25, and 40 wt.% of BMW (F2 to F8) after sintering treatments (1150, 1200, and 1250 °C).

For the samples with BMW (F2 to F8), the increase in FS values with increasing temperature is more discrete, except sample F6 (with 20 wt.% BMW), which showed a slight decrease. This behavior can be attributed to the higher content of fluxing oxides present in the waste, which favors the formation of a liquid phase at lower temperatures. From 1200 °C to 1250 °C, the mechanical strength increases only for F3 (with 5 wt.% BMW) and decreases slightly in the other samples. The highest FS value (37.92 MPa) was reached for sample F8 (with 40 wt.% BMW) sintered at 1200 °C. Therefore, according to the requirements determined by the standard ISO 13006 [53], all samples sintered at 1150 °C and containing between 5 and 40 wt.% of bentonite waste can be used as semi-stoneware (WA values between 3.0% and 6.0% and FS ≥ 22 MPa); those with 10 to 40 wt.% of BMW and sintered at 1200 °C as stoneware (WA values in the range of 0.5–3.0% and FS ≥ 30 MPa) and, finally, F3 (5 wt.% BMW), F7 (25 wt.% BMW) and F8 (40 wt.% BMW) sintered at 1250 °C as porcelain stoneware for presenting WA values ≤ 0.5% and FS ≥ 35 MPa.

3.5. Mineralogical Phases and Morphology of the Samples after Sintering

The XRD patterns of the samples sintered at 1250 °C are shown in Figure 9. It is possible to observe that, for all samples, only the mullite (JCPDS 79-1276) and quartz were detected. A decrease in the intensity of the main quartz peak ($2\theta = 26.64°$) was observed with the addition of BMW, which was expected since the bentonite waste was incorporated into the standard formulation as a substitute for quartz and a partial for feldspar. Regarding the samples containing bentonite waste (F2 to F8), the patterns practically show identical peaks, which indicates that the increase in the BMW content (up to 40 wt.%) did not cause considerable changes in the mineralogical profile of the samples. Mullite forms a network of needle-shaped structures responsible for increasing the material's strength [55,56]. At $2\theta = 20–30°$, the glass phase is a characteristic halo [20,57].
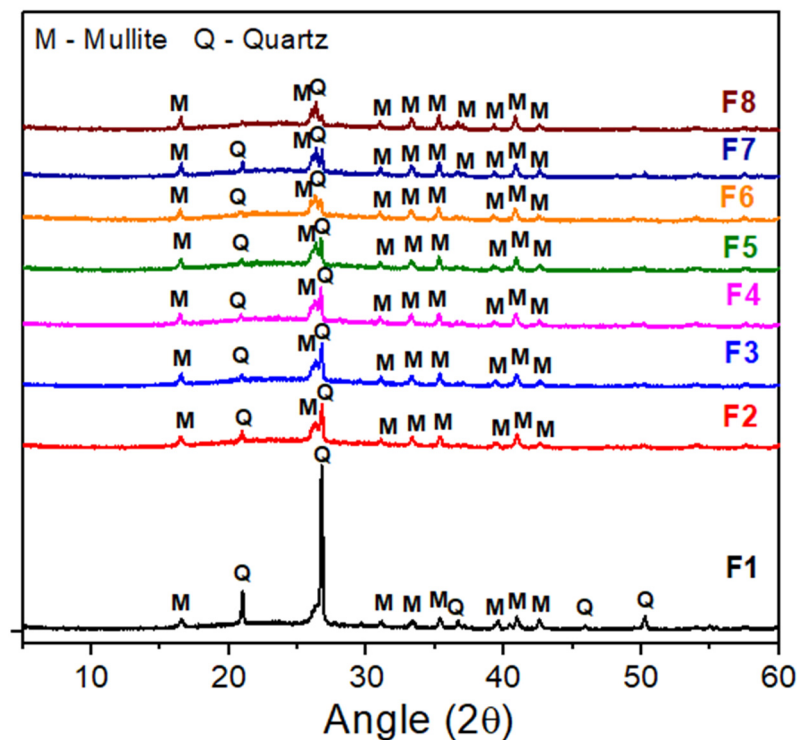
Figure 9. XRD patterns were measured from samples without the BMW (F1) and with 2.5, 5, 10, 15, 20, 25, and 40 wt.% of the BMW (F2 to F8) after sintering treatment at 1250 °C.

The morphology of sintered samples sintered at 1250 °C was investigated by SEM micrographics. Figure 10 shows SEM images acquired from the surface of the samples. The surface is dense and vitrified in all samples with small, isolated pores. It is observed that the microstructure is characterized by an abundant amount of glass phase and some small needle-like crystals (squares highlighted in red in the images). These crystals are of mullite, which develops and form a network of intertwined needles that contribute to the increase in the material's strength. Mullite is formed from the dissolution and crystallization of the aluminosilicate present in the liquid phase. During this process, aluminum ions react with silicon ions from the amorphous phase (rich in SiO_2), promoting the growth of mullite crystals [58,59]. The mullite formation process can be accelerated by the action of impurity present, such as Fe_2O_3, TiO_2, K_2O, and Na_2O [58,60]. The small spherical grains can be attributed to the residual quartz phase (circles highlighted in yellow in the images). These results corroborate the X-ray analysis, which indicates mullite and quartz as the main crystalline phases.
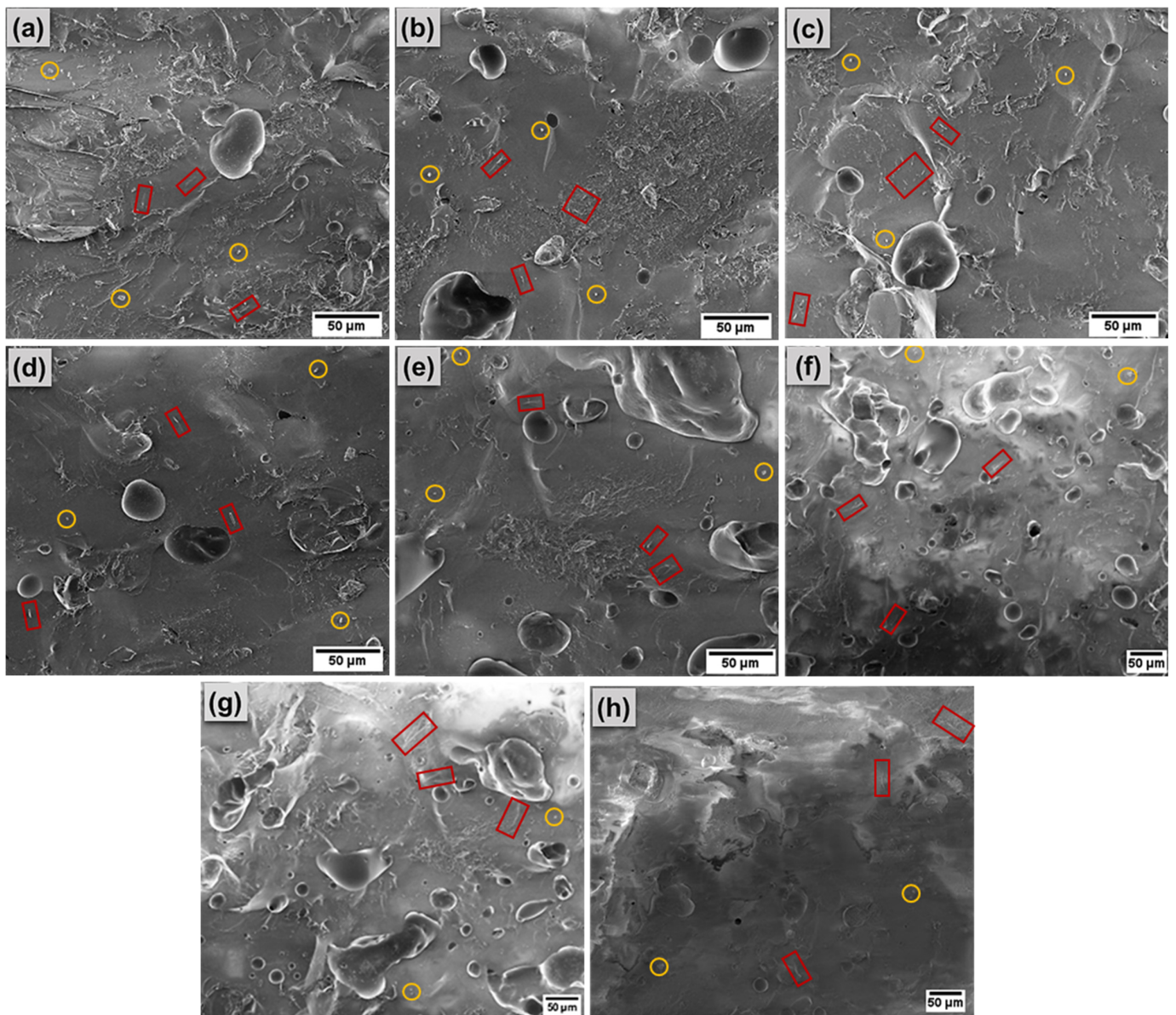
Figure 10. SEM images were acquired from samples sintered at 1250 °C. (**a**) F1, (**b**) F2, (**c**) F3, (**d**) F4, (**e**) F5, (**f**) F6, (**g**) F7, and (**h**) F8. In the Figures, the red squares refer to the mullite crystals and the yellow circles are attributed to the residual quartz.

4. Conclusions

Based on the results of this study, the waste from bentonite mining can be used as an alternative raw material for producing porcelain stoneware, as a substitute for quartz, and partially for feldspar. The bentonite mining waste showed adequate chemical composition and granulometric distribution for use in ceramic mass. The incorporation of the bentonite waste and the increase in the sintering temperature favored the reduction in the water absorption and porosity and the growth of the flexural strength of the samples. Regardless of the sintering temperature, the sample without bentonite waste showed the highest water absorption values and lowered flexural strength than the samples with the waste. The samples with waste percentages above 15 wt.% (F5, F6, F7, and F8) showed flexural strength >30 MPa, with the highest value (37.92 MPa) reached for the sample with 40 wt.% waste and sintered at 1200 °C. The X-ray diffraction patterns of the samples sintered at 1250 °C indicated mullite and quartz as the main crystalline phases. SEM images from samples revealed mullite crystals amid the glass phase and small spherical grains attributed to

the residual quartz phase. In general, based on the standard ISO 13006 [54], all samples that were sintered at 1150 °C and contained between 5 and 40 wt.% of bentonite waste showed potential to be used as semi-stoneware; those with 10 to 40 wt.% sintered at 1200 °C as stoneware and those with 5, 25, and 40 wt.% of waste sintered at 1250 °C as porcelain stoneware.

References

1. Brazilian Mining Association—IBRAM: Mineral Sector 2021. Available online: https://ibram.org.br/ (accessed on 7 October 2022).
2. Muhammad, N.; Siddiqua, S. Calcium Bentonite vs Sodium Bentonite: The Potential of Calcium Bentonite for Soil Foundation. *Mater. Today Proc.* **2022**, *48*, 822–827. [CrossRef]
3. Magzoub, M.I.; Nasser, M.S.; Hussein, I.A.; Benamor, A.; Onaizi, S.A.; Sultan, A.S.; Mahmoud, M.A. Effects of Sodium Carbonate Addition, Heat and Agitation on Swelling and Rheological Behavior of Ca-Bentonite Colloidal Dispersions. *Appl. Clay Sci.* **2017**, *147*, 176–183. [CrossRef]
4. Chakraborty, S.; Anoop, V.; George, N.; Bhagyasree, T.; Mary, N.L. Physicochemical Stability Evaluation of Cosmetic Formulations of PVA, Starch and MMT Clay Nanocomposites. *SN Appl. Sci.* **2019**, *1*, 581. [CrossRef]
5. Cavalcanti, R.K.B.C.; Brasileiro, C.T.; Macedo, R.O.; Ferreira, H.S. Mineral Make up Developed from Natural and Organophilic Bentonite Clays. *Ceramica* **2018**, *64*, 266–275. [CrossRef]
6. Dardir, F.M.; Mohamed, A.S.; Abukhadra, M.R.; Ahmed, E.A.; Soliman, M.F. Cosmetic and Pharmaceutical Qualifications of Egyptian Bentonite and Its Suitability as Drug Carrier for Praziquantel Drug. *Eur. J. Pharm. Sci.* **2018**, *115*, 320–329. [CrossRef] [PubMed]
7. Martsouka, F.; Papagiannopoulos, K.; Hatziantoniou, S.; Barlog, M.; Lagiopoulos, G.; Tatoulis, T.; Tekerlekopoulou, A.G.; Lampropoulou, P.; Papoulis, D. The Antimicrobial Properties of Modified Pharmaceutical Bentonite with Zinc and Copper. *Pharmaceutics* **2021**, *13*, 1190. [CrossRef]
8. Magzoub, M.; Mahmoud, M.; Nasser, M.; Hussein, I.; Elkatatny, S.; Sultan, A. Thermochemical Upgrading of Calcium Bentonite for Drilling Fluid Applications. *J. Energy Resour. Technol. Trans. ASME* **2019**, *141*, 042902. [CrossRef]
9. Zhang, J.; Xu, M.; Christidis, G.; Zhou, C. Clay Minerals in Drilling Fluids: Functions and Challenges. *Clay Miner.* **2020**, *55*, 1–11. [CrossRef]
10. Rizzi, V.; Gubitosa, J.; Fini, P.; Romita, R.; Agostiano, A.; Nuzzo, S.; Cosma, P. Commercial Bentonite Clay as Low-Cost and Recyclable "Natural" Adsorbent for the Carbendazim Removal/Recover from Water: Overview on the Adsorption Process and Preliminary Photodegradation Considerations. *Colloids Surfaces A Physicochem. Eng. Asp.* **2020**, *602*, 125060. [CrossRef]
11. Khalilzadeh Shirazi, E.; Metzger, J.W.; Fischer, K.; Hassani, A.H. Removal of Textile Dyes from Single and Binary Component Systems by Persian Bentonite and a Mixed Adsorbent of Bentonite/Charred Dolomite. *Colloids Surfaces A Physicochem. Eng. Asp.* **2020**, *598*, 124807. [CrossRef]
12. Visentin, C.; Zanella, P.; Kronhardt, B.K.; da Trentin, A.W.S.; Braun, A.B.; Thomé, A. Use of Geosynthetic Clay Liner as a Waterproofing Barrier in Sanitary Landfills. *J. Urban Environ. Eng.* **2019**, *13*, 115–124. [CrossRef]
13. Resumo Mineral Do Estado da Paraíba. Available online: http://www.cinep.pb.gov.br/ (accessed on 7 October 2022).
14. Alves, J.L.; Zanini, A.E.; de Souza, M.E.; Nascimento, M.L.F. Study of Selection and Purification of Brazilian Bentonite Clay by Elutriation: A XRF, SEM and Rietveld Analysis. *Cerâmica* **2016**, *62*, 1–8. [CrossRef]

15. Ribeiro, A.; Kroetz, B.L.; Tarley, C.R.T.; Abrao, T.; Parreira, P.S.; Santos, M.J. Separating Selenium Species by Diffusion in Brazilian Bentonite: A Mathematical Modeling Approach. *Environ. Sci. Pollut. Res.* **2022**, *29*, 88119–88130. [CrossRef] [PubMed]

16. Cota, T.; Reis, E.; Lima, R.; Cipriano, R.A.S. Incorporation of Waste from Ferromanganese Alloy Manufacture and Soapstone Powder in Red Ceramic Production. *Appl. Clay Sci.* **2018**, *161*, 274–281. [CrossRef]

17. De Almeida, E.P.; de Brito, I.P.; Ferreira, H.C.; de Lira, H.L.; de Lima Santana, L.N.; de Araújo Neves, G. Cordierite Obtained from Compositions Containing Kaolin Waste, Talc and Magnesium Oxide. *Ceram. Int.* **2018**, *44*, 1719–1725. [CrossRef]

18. de Brito, I.P.; de Almeida, E.P.; de Araújo Neves, G.; de Lucena Lira, H.; Menezes, R.R.; da Silva, V.J.; de Lima Santana, L.N. Development of Cordierite/Mullite Composites Using Industrial Wastes. *Int. J. Appl. Ceram. Technol.* **2021**, *18*, 253–261. [CrossRef]

19. Fernandes, J.V.; Guedes, D.G.; da Costa, F.P.; Rodrigues, A.M.; de Neves, G.A.; Menezes, R.R.; Santana, L.N.d.L. Sustainable Ceramic Materials Manufactured from Ceramic Formulations Containing Quartzite and Scheelite Tailings. *Sustainability* **2020**, *12*, 9417. [CrossRef]

20. De Figueirêdo, J.M.R.; da Costa, F.P.; Fernandes, J.V.; Rodrigues, A.M.; de Neves, G.A.; Menezes, R.R.; Santana, L.N.d.L. Development of Scheelite Tailings-Based Ceramic Formulations with the Potential to Manufacture Porcelain Tiles, Semi-Stoneware and Stoneware. *Materials* **2020**, *13*, 5122. [CrossRef]

21. Fontes, W.C.; Franco de Carvalho, J.M.; Andrade, L.C.R.; Segadães, A.M.; Peixoto, R.A.F. Assessment of the Use Potential of Iron Ore Tailings in the Manufacture of Ceramic Tiles: From Tailings-Dams to "Brown Porcelain". *Constr. Build. Mater.* **2019**, *206*, 111–121. [CrossRef]

22. Marrocchino, E.; Zanelli, C.; Guarini, G.; Dondi, M. Recycling Mining and Construction Wastes as Temper in Clay Bricks. *Appl. Clay Sci.* **2021**, *209*, 106152. [CrossRef]

23. Loutou, M.; Taha, Y.; Benzaazoua, M.; Daafi, Y.; Hakkou, R. Valorization of Clay By-Product from Moroccan Phosphate Mines for the Production of Fired Bricks. *J. Clean. Prod.* **2019**, *229*, 169–179. [CrossRef]

24. Vilela, A.P.; Eugênio, T.M.C.; de Oliveira, F.F.; Mendes, J.F.; Ribeiro, A.G.C.; de Brandão Vaz, L.E.V.S.; Mendes, R.F. Technological Properties of Soil-Cement Bricks Produced with Iron Ore Mining Waste. *Constr. Build. Mater.* **2020**, *262*, 120883. [CrossRef]

25. Benahsina, A.; Taha, Y.; Bouachera, R.; Elomari, M.; Bennouna, M.A. Manufacture and Characterization of Fired Bricks from Gold Mine Waste Rocks. *Minerals* **2021**, *11*, 695. [CrossRef]

26. Benahsina, A.; El Haloui, Y.; Taha, Y.; Elomari, M.; Bennouna, M.A. Substitution of Natural Clay by Moroccan Solid Mining Wastes to Manufacture Fired Bricks. *Mater. Today Proc.* **2022**, *58*, 1324–1330. [CrossRef]

27. Carvalho Eugênio, T.M.; Francisco Fagundes, J.; Santos Viana, Q.; Pereira Vilela, A.; Farinassi Mendes, R. Study on the Feasibility of Using Iron Ore Tailing (Iot) on Technological Properties of Concrete Roof Tiles. *Constr. Build. Mater.* **2021**, *279*, 122484. [CrossRef]

28. Veiga Simão, F.; Chambart, H.; Vandemeulebroeke, L.; Cappuyns, V. Incorporation of Sulphidic Mining Waste Material in Ceramic Roof Tiles and Blocks. *J. Geochemical Explor.* **2021**, *225*, 106741. [CrossRef]

29. Ahmed, M.M.; Abadir, M.; Yousef, A.; El-Naggar, K.A.M. The Use of Aluminum Slag Waste in the Preparation of Roof Tiles. *Mater. Res. Express* **2021**, *8*, 125501. [CrossRef]

30. Almeida, E.P.; Carreiro, M.E.A.; Rodrigues, A.M.; Ferreira, H.S.; Santana, L.N.L.; Menezes, R.R.; Neves, G.A. A New Eco-Friendly Mass Formulation Based on Industrial Mining Residues for the Manufacture of Ceramic Tiles. *Ceram. Int.* **2021**, *47*, 11340–11348. [CrossRef]

31. Wang, W.; Chen, W.; Liu, H. Recycling of Waste Red Mud for Fabrication of SiC/Mullite Composite Porous Ceramics. *Ceram. Int.* **2019**, *45*, 9852–9857. [CrossRef]

32. Da Silva, V.J.; da Silva, M.F.; Gonçalves, W.P.; de Menezes, R.R.; de Araújo Neves, G.; de Lucena Lira, H.; de Lima Santana, L.N. Porous Mullite Blocks with Compositions Containing Kaolin and Alumina Waste. *Ceram. Int.* **2016**, *42*, 15471–15478. [CrossRef]

33. Da Costa, F.P.; da Morais, C.R.S.; Rodrigues, A.M. Sustainable Glass-Ceramic Foams Manufactured from Waste Glass Bottles and Bentonite. *Ceram. Int.* **2020**, *46*, 17957–17961. [CrossRef]

34. Da Costa, F.P.; da Morais, C.R.S.; Pinto, H.C.; Rodrigues, A.M. Microstructure and Physico-Mechanical Properties of Al2O3-Doped Sustainable Glass-Ceramic Foams. *Mater. Chem. Phys.* **2020**, *256*, 123612. [CrossRef]

35. De Medeiros, P.S.S.; Lira, H.D.L.; Rodriguez, M.A.; Menezes, R.R.; Neves, G.D.A.; Santana, L.N.D.L. Incorporation of Quartzite Waste in Mixtures Used to Prepare Sanitary Ware. *J. Mater. Res. Technol.* **2019**, *8*, 2148–2156. [CrossRef]

36. Ferreira, I.C.; Galéry, R.; Henriques, A.B.; Paula De Carvalho Teixeira, A.; Prates, C.D.; Lima, A.S.; Souza Filho, I.R. Reuse of Iron Ore Tailings for Production of Metakaolin-Based Geopolymers. *J. Mater. Res. Technol.* **2022**, *18*, 4194–4200. [CrossRef]

37. Goulart Bezerra, C.; Abelha Rocha, C.A.; de Siqueira, I.S.; Toledo Filho, R.D. Feasibility of Iron-Rich Ore Tailing as Supplementary Cementitious Material in Cement Pastes. *Constr. Build. Mater.* **2021**, *303*, 124496. [CrossRef]

38. HK, T.; Hossiney, N. A Short Review on Environmental Impacts and Application of Iron Ore Tailings in Development of Sustainable Eco-Friendly Bricks. *Mater. Today Proc.* **2022**, *61*, 327–331. [CrossRef]

39. Rodrigues, A.M.; da Costa, F.P.; Beltrão, S.L.D.; Fernandes, J.V.; Menezes, R.R.; Neves, G.d.A. Development of Eco-Friendly Mortars Produced with Kaolin Processing Waste: Durability Behavior Viewpoint. *Sustainability* **2021**, *13*, 11395. [CrossRef]

40. da Silva, M.R.C.; Malacarne, C.S.; Longhi, M.A.; Kirchheim, A.P. Valorization of Kaolin Mining Waste from the Amazon Region (Brazil) for the Low-Carbon Cement Production. *Case Stud. Constr. Mater.* **2021**, *15*, e00756. [CrossRef]

41. Carreiro, M.E.A.; da Silva, V.J.; Rodrigues, A.M.; de Barbosa, E.P.A.; da Costa, F.P.; Menezes, R.R.; Neves, G.A.; Santana, L.N.d.L. Firing Parameters Effect on the Physical and Mechanical Properties of Scheelite Tailings-Containing Ceramic Masses. *Sustainability* **2022**, *14*, 333. [CrossRef]

42. Souza, M.M.; Anjos, M.A.S.; Sá, M.V.V.A. Using Scheelite Residue and Rice Husk Ash to Manufacture Lightweight Aggregates. *Constr. Build. Mater.* **2021**, *270*, 121845. [CrossRef]

43. Barbosa, M.Z.; de Oliveira Dias, J.; Marvila, M.T.; de Azevedo, A.R.G. Life Cycle Approach Applied to the Production of Ceramic Materials Incorporated with Ornamental Stone Wastes. *Environ. Sci. Pollut. Res.* **2022**, *29*, 9957–9970. [CrossRef] [PubMed]

44. Paes, A.L.; Alexandre, J.; de Xavier, G.C.; Monteiro, S.N.; de Azevedo, A.R.G. Feasibility Analysis of Mortar Development with Ornamental Rock Waste for Coating Application by Mechanized Projection. *Sustainability* **2022**, *14*, 5101. [CrossRef]

45. De Oliveira Neto, R.E.; de Cartaxo, J.M.; Rodrigues, A.M.; Barros, S.V.A.; da Costa, F.P.; de Neves, G.A.; Menezes, R.R. New Sustainable Mortar Compositions Containing Perlite Waste. *Clean Technol. Environ. Policy* **2022**, *24*, 1403–1415. [CrossRef]

46. Abed, M.; Fořt, J.; Rashid, K. Multicriterial Life Cycle Assessment of Eco-Efficient Self-Compacting Concrete Modified by Waste Perlite Powder and/or Recycled Concrete Aggregate. *Constr. Build. Mater.* **2022**, *348*, 128696. [CrossRef]

47. Fabien, A.; Sebaibi, N.; Boutouil, M. Effect of Several Parameters on Non-Autoclaved Aerated Concrete: Use of Recycling Waste Perlite. *Eur. J. Environ. Civ. Eng.* **2022**, *26*, 58–75. [CrossRef]

48. Evaristo De Oliveira Neto, R.; De Melo Cartaxo, J.; Mendes Rodrigues, A.; De Araújo Neves, G.; Rodrigues Menezes, R.; Pereira Da Costa, F.; Valensca, S.; Barros, A. Durability Behavior of Mortars Containing Perlite Tailings: Alkali-Silicate Reaction Viewpoint. *Sustainability* **2021**, *13*, 9203. [CrossRef]

49. Araújo, M.E.B.; Silva, V.C.; Fernandes, J.V.; Cartaxo, J.M.; Rodrigues, A.M.; Menezes, R.R.; de Araújo Neves, G. Innovative Adsorbents Based on Bentonite Mining Waste for Removal of Cationic Dyes from Wastewater. *Environ. Sci. Pollut. Res.* **2022**, 1–17. [CrossRef]

50. *ISO Internacional ISO 10545-3*; Ceramic Tiles—Part 3: Determination of Water Absorption, Apparent Porosity, Apparent Relative Density and Bulk Density. Turkish Standards Institution: Ankara, Turkey, 2014.

51. Pazniak, A.; Barantseva, S.; Kuzmenkova, O.; Kuznetsov, D. Effect of Granitic Rock Wastes and Basalt on Microstructure and Properties of Porcelain Stoneware. *Mater. Lett.* **2018**, *225*, 122–125. [CrossRef]

52. Brasileiro, C.T.; de Filho, H.D.A.; Santana, G.L.; Lot, A.V.; Conte, S.; Zanelli, C.; Dondi, M.; Boschi, A.O. Sericite Instead of Feldspar in Porcelain Stoneware: Effect on Sintering and Phase Evolution. *Int. J. Appl. Ceram. Technol.* **2022**, *19*, 612–622. [CrossRef]

53. *ISO Internacional ISO 13006:2018*; Ceramic Tiles—Definitions, Classification, Characteristics and Marking. International Organization for Standardization: Geneva, Switzerland, 2018.

54. Issaoui, M.; Limousy, L.; Lebeau, B.; Bouaziz, J.; Fourati, M. Design and characterization of flat membrane supports elaborated from kaolin and aluminum powders. *C. R. Chim.* **2016**, *19*, 496–504. [CrossRef]

55. Huo, W.; Zhang, X.; Chen, Y.; Hu, Z.; Wang, D.; Yang, J. Ultralight and High-Strength Bulk Alumina/Zirconia Composite Ceramic Foams through Direct Foaming Method. *Ceram. Int.* **2019**, *45*, 1464–1467. [CrossRef]

56. da Silva, V.J.; Taveira, S.K.A.; Silva, K.R.; Neves, G.A.; Lira, H.L.; Santana, L.N.L. Refractory Ceramics of Clay and Alumina Waste. *Mater. Res.* **2021**, *24*, e20200485. [CrossRef]

57. Ochen, W.; D'ujanga, F.M.; Oruru, B.; Olupot, P.W. Physical and Mechanical Properties of Porcelain Tiles Made from Raw Materials in Uganda. *Results Mater.* **2021**, *11*, 100195. [CrossRef]

58. Karhu, M.; Lagerbom, J.; Solismaa, S.; Honkanen, M.; Ismailov, A.; Räisänen, M.L.; Huttunen-Saarivirta, E.; Levänen, E.; Kivikytö-Reponen, P. Mining Tailings as Raw Materials for Reaction-Sintered Aluminosilicate Ceramics: Effect of Mineralogical Composition on Microstructure and Properties. *Ceram. Int.* **2019**, *45*, 4840–4848. [CrossRef]

59. Hou, Z.; Cui, B.; Liu, L.; Liu, Q. Effect of the Different Additives on the Fabrication of Porous Kaolin-Based Mullite Ceramics. *Ceram. Int.* **2016**, *42*, 17254–17258. [CrossRef]

60. Xu, X.; Li, J.; Wu, J.; Tang, Z.; Chen, L.; Li, Y.; Lu, C. Preparation and Thermal Shock Resistance of Corundum-Mullite Composite Ceramics from Andalusite. *Ceram. Int.* **2017**, *43*, 1762–1767. [CrossRef]